Atmospheric Pollution Research xxx (xxxx) xxx

Contents lists available at ScienceDirect

Atmospheric Pollution Research

journal homepage: www.elsevier.com/locate/apr

Assessment of pollutant dispersion in urban street canyons based on field synergy theory

Tingzhen Ming [a,b], Tianhao Shi [a], Huina Han [a], Shurong Liu [a], Yongjia Wu [a], Wenyu Li [c], Chong Peng [d,*]

[a] School of Civil Engineering and Architecture, Wuhan University of Technology, No. 122, Luoshi Road, Wuhan, 430070, China
[b] School of Architectural Engineering, Huanggang Normal University, No. 146 Xingang Second Road, Huanggang, 438000, China
[c] Department of Mechanical Engineering, University of California at Berkeley, CA, 94720-1740, USA
[d] School of Architecture and Urban Planning, Huazhong University of Science and Technology, No.1037, Luoyu Road, Hongshan District, Wuhan, 430074, China

ARTICLE INFO

Keywords:
Street canyon
Field synergy theory
Numerical simulation
Pollutant dispersion

ABSTRACT

Vehicle emissions are an important factor in the deterioration of air quality in urban street canyons. To improve the air quality in urban street canyons, it is necessary to have a deep understanding of the mechanism of pollutant dispersion within the urban boundary layer. The transport process of pollutants in street canyons is essentially a convective mass transfer process. In this paper, a computational fluid dynamics (CFD) simulation is conducted to investigate the effects of wind speed, the setting of the viaduct, and the roof shapes of the street canyons on pollutant dispersion. According to the field synergy theory, Sherwood number and field synergy number are used to evaluate the three factors on the diffusion of pollutants in street canyons quantitatively. The results show that the Sherwood number decreases with increased viaduct construction height and decreased wind speed, which is compatible with the observed growth of pollutant fraction in the street canyon. When the pollution source on the viaduct is considered, a less substantial influence of construction height on pollutant diffusion is observed. Among the four types of roofs, upward pitched roofs resulted in the highest pollution, with a pollution concentration degree of 1.6–2.3 times that of flat roofs, followed by double pitched roofs, with a pollution concentration degree of 1.2–2 times that of a flat roof. By the method of analogy analysis and numerical simulation, the field synergy theory has been extended from applications in heat transfer in small-scale confined spaces to those in urban street canyon pollution simulation in large-scale open spaces.

1. Introduction

As the process of economic globalization continues to accelerate, people's living standards are increasing as well. The urban building density grows constantly due to accelerated urbanization, leading to a declined urban ventilation rate. Motor vehicles have gradually become a necessity for people to travel, and the surge in the number of vehicles and the amount of traffic congestion has become the main contributor to air pollution in urban blocks. Lu et al. (2019) found that traffic pollution in the air is very harmful to human health and may even cause preterm birth. Therefore, it is critical to improve the environmental quality of urban blocks.

The concept of the street canyon was introduced initially by Nicholson (Nicholson, 1975): it is composed of two buildings arranged continuously on both sides of a street. As the main area for human activities, the street canyon microenvironment has attracted increased attention from researchers. According to the literature, impact of different factors on the environmental quality of urban street canyons has been investigated through on-site measurements, wind tunnel tests, and numerical simulations. The influencing factors can be roughly divided into three categories: (1) Urban street canyon morphology, including street canyon aspect ratio (the ratio of building height to street width, *H/W*) (Assimakopoulos et al., 2003), geometric symmetry or asymmetry (Gu et al., 2011), building roof shape (Kastner et al., 2004; Xie et al., 2005a, 2005b), obstruction of facilities in the street canyon such as vegetation (Nowak et al., 2006; Tallis et al., 2011; Su et al., 2019), viaducts (Hao et al., 2019; Hang et al., 2019), low walls (Dou et al., 2018), etc. (2) Meteorological conditions, for example wind speed and direction (Kim and Baik, 2004; Soulhac et al., 2008), and thermal effects caused by solar radiation (Xie et al., 2005a, 2005b; Tan et al., 2015; Lin et al., 2016; Dong et al., 2017). (3) Turbulent kinetic energy

* Corresponding author.
E-mail address: pengchong@hust.edu.cn (C. Peng).

https://doi.org/10.1016/j.apr.2020.11.015
Received 17 August 2020; Received in revised form 23 November 2020; Accepted 23 November 2020
Available online 8 December 2020

Nomenclature

ACH	air exchange rate
PCH	pollution exchange rate
PFR	purging flow rate
NEV	net escape velocity
P_IF	personal intake fraction
CPL	capillary pumped loop
$\vec{U}$	velocity vector
∇T	temperature gradient
∇C	concentration gradient
μ	dynamic viscosity
S_c	Schmidt number
ρ	air density
λ	thermal conductivity
Ω	flow domain
DS	double source
x,y,z	Cartesian coordinates
Re	Reynolds number
V	volume
Nu	Nusselt number
c_p	specific heat capacity at constant pressure
q	strength of heat source
q_w	wall heat flux
T	temperature
T_w	wall temperature
T_∞	free-stream fluid temperature
$\overrightarrow{\overline{U}}$	dimensionless velocity vector
$\nabla\overline{T}$	dimensionless temperature gradient
$\overline{\nabla C}$	dimensionless concentration gradient
$\delta_{t,x}$	thermal boundary layer thickness
D	mass diffusion coefficient
$\vec{n}$	outward normal unit vector
S_h	Sherwood number
SS	single source
u	velocity component along x-coordinate
v	velocity component along y-coordinate
P_r	Prandtl number
ν	dynamic viscosity

caused by vehicle movement (Jicha et al., 2000; Ahmad et al., 2002; Solazzo et al., 2008; Li et al., 2017, 2020; Wang et al., 2019), secondary pollution caused by photochemical reaction (Baik et al., 2006; Merah and Noureddine, 2019), the shape of the pollution source (Tan et al., 2019), etc.

From the literature review, it is found that the urban ambient wind speed, the setting of viaducts, and the shape of building roofs have an important impact on the pollutants dispersion in urban street canyons. Hao et al. (2019) investigated the effects of viaducts on the flow pattern and particle diffusion in street canyons. The results demonstrated that viaducts induce more sources of particulate and have a greater impact on flow patterns. Ding et al. (2019) investigated the influence of the height of viaducts in the streets with different roofs on the flow field and the diffusion of pollutants. The study showed that the obstruction of the viaduct caused an inverse flow, which aggravated the pollution in the street canyon with the double flat roof and reduced the pollution with the double slope roof. Hang et al. (2018) examined the impact of viaduct setting on personal intake fraction and found that viaduct and noise barrier can substantially affect the vortex center and pollutant diffusion mode; the location of the pollution source is also a key factor affecting pollutant dispersion. The influence of roof shape on the flow field and pollutant diffusion in the street canyon was investigated by Takano and Moonen (2013). The results showed that the roof slope can change the vortex structure in the street canyon. In the single vortex state, the pollutant concentration decreased with increased roof slope. In the double vortex state, limited mixing occurred between the two vortex cores, resulting in a higher concentration of pollutants near the ground. Huang et al. (2015) studied the influence of five shapes of upstream roofs with various heights on the diffusion of pollutants. The results showed that the concentration of pollution with upward wedged roof and slanted roof were much higher than other roofs at $Z_H/H = 1/3$ (the ratios of roof height to building height); the lowest and highest pollution levels were observed for vaulted roof and upward wedged roof at $Z_H/H = 1/2$, respectively. However, previous work focused on qualitatively describing the diffusion of pollutants and a quantitative evaluation for the impact of different factors is lacking and necessary.

Some indicators useful to characterize the ventilation and pollutant dispersion effect in street canyons have been defined by predecessors, and include the air exchange rate (ACH), pollution exchange rate (PCH), purging flow rate (PFR), net escape velocity (NEV), pollutant residence time or decay time, and personal intake fraction (P_IF). According to Liu et al. (2005), the ACH and PCH were defined as the amount of air and air pollutants entering and leaving the street canyon from the top of street canyon per unit time. However, while the ACH and PCH reflect the rate of air or pollutants entering and exiting the street canyon, they cannot reflect the proportion and distance of air transported to the bottom of the street canyon. Kato et al. (2003) defined the PFR, which represents the amount of air needed to dilute pollutants in the target computing domain per unit time, and reflects the overall ventilation efficiency of the street canyon. However, the PFR is related to geometric size. Later, Hang et al. (2015) proposed to use the PFR/boundary area, that is, the NEV, to eliminate the effect of size, and pointed out that NEV_{ped} represents the net capacity to dilute pedestrian-level pollutants with the average flow and turbulent diffusion. Cheng et al. (2008) and Li et al. (2008) used the average time that the pollutants stay in the target area to evaluate the air pollution diffusion capacity of street canyons. Caton et al. (2003) evaluated the street canyon pollution removal capacity via the time required for the concentration to decay to 1/e after the pollutant discharge stops. Baratian and Kaye (2013) evaluated the pollution removal capacity in street canyons via the time required to reduce the concentration of pollutants to 10% of the original concentration. In summary, the NEV and pollutant residence time can effectively reflect the diffusion capacity of pollutants in street canyons. Hang et al. (2017) defined the individual intake ratio (P_IF), multiplied it by the average concentration of a specific micro-environment within one day to estimate daily CO exposure, and used this estimation to assess street canyon environmental quality. However, at present, there remains a lack of attention paid to the basic theory that the diffusion of pollutants in street canyons is a process of convective mass diffusion under the effect of ambient wind. This work investigates the law of pollutant dispersion in urban street canyons from this aspect.

To improve the environmental quality in street canyons, it is necessary to enhance the diffusion capacity of pollutants in street canyons, i.e., the convective mass transfer process needs to be strengthened. Mass transfer is a mass diffusion process caused by a concentration gradient, which is analogous to heat transfer (Chen et al., 2008). The enhanced heat transfer field synergy theory is a well-established theory for guiding improved heat transfer. Guo et al. (1998) compared convective heat transfer to a heat conduction problem with an internal heat source, proposed the concept of source enhancement and deduced the field synergy principle of heat transfer enhancement by integrating the boundary layer energy equation. Zeng and Tao (2004) applied the

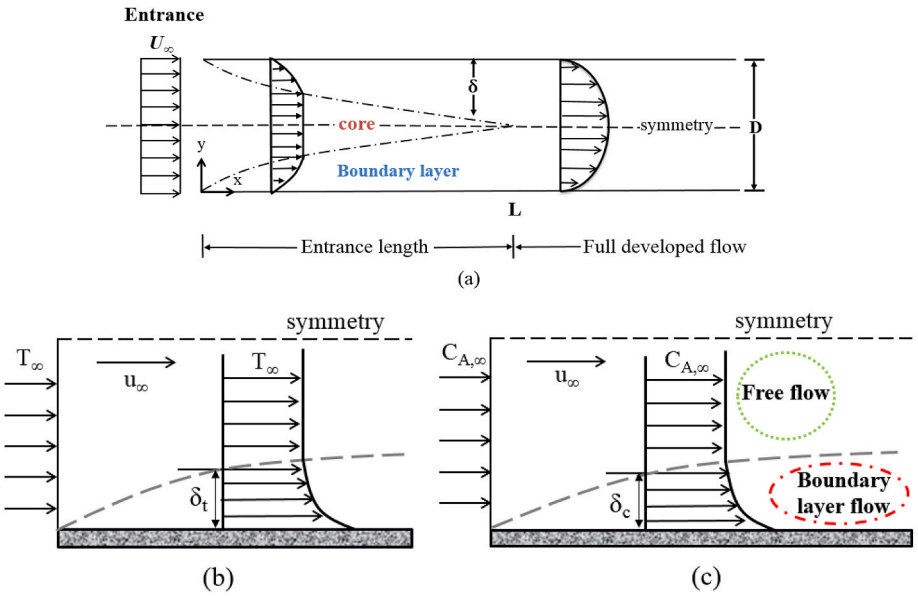

Fig. 1. (a) Developing flow in the entrance region of the duct formed between two parallel plates (modified from Bejan, 1984.); (b) diagram of temperature boundary layer; and (c) diagram of concentration boundary layer.

field synergy principle of heat transfer to turbulent flow, and proved that the field synergy principle of heat transfer is also applicable to turbulent flow. Liu et al. (2010) established a synergy equation of energy and momentum for turbulent heat transfer, which revealed the synergy between heat flow, mass flow, and fluid in driving force during turbulent heat transfer. The results proved the applicability of the field synergy principle in turbulent heat transfer. Motivated by the analogy among momentum transfer, heat transfer, and mass transfer, the field synergy theory has been extended to the field of convective mass transfer. Based on the analogy of the three transmission processes, Chen et al. (2008) extended the field synergy principle to the analysis of convection mass transfer, and revealed the influence of the synergy between the velocity vector and the pollutant concentration gradient on the decontamination rate of indoor ventilation. The best ventilation method was obtained by solving the field synergy equation, which improves the room purification ability and provides theoretical guidance for using the field synergy principle to improve the indoor decontamination rate.

In summary, the field synergy theory can be extended to the field of convective mass transfer, and its applicability in turbulent flow has also been proven. However, until now, the research on field synergy theory has only been applied in confined spaces. For example, Tao et al. (2002) studied the convective heat transfer in discrete plates, wavy channels, and corrugate ducts, and then verified the effectiveness of the field synergy principle. Liu et al. (2007) carried out a numerical study on the flow and heat transfer characteristics in the porous core of a CPL evaporator based on the field synergy principle to analyze the effects of geometric structure and heat flux density on heat transfer enhancement. Liu et al. (2012) evaluated the performance of enhanced convective heat transfer in a circular tube by applying the multi-field synergy principle.

In this work, we take the urban street canyon as the research object and prove the applicability of the field synergy theory in the study of pollutant transmission in open space via the method of model similarity. Then the theory is applied for analyzing pollution dispersion in urban street canyons. The Sherwood number and the field synergy number are used to evaluate the quality of pollutant dispersion capacity in the street canyons for different factors, e.g., the setting of the viaduct, the wind speed and the roof shape. Based on field synergy theory, the internal relationship between the pollutant dispersion capacity in the street canyon and the effect of convective mass transfer is then revealed.

2. The analogy among momentum transfer, heat transfer, and mass transfer

Fig. 1a presents the laminar flow through a two-dimensional duct formed between two parallel plates. The spacing between the plates is *D*. Boundary layers grow along the *x*-axis until they meet at location $x \approx$ L downstream from the entrance, where the length L is termed entrance length. In the flow entrance region, the flow is divided into the boundary layer flow and the core flow. There is an observable velocity gradient inside the boundary layer, in which the velocity decreases toward the wall. The velocity in the core flow region is basically constant. The flow between the two parallel plates is symmetric about the centerline. Therefore, we can take the half domain as the simulation object in the numerical study and use the symmetry boundary condition. The half domain simulation is similar to that in the semi-confined space structure, for example, the fluid flows through a plate. In the numerical simulation study of street canyon pollution, the height of the computation domain is generally set to at least 6 times the height of the buildings (Mochida et al., 2002; Shirasawa et al., 2003; Yoshihide et al.2008), so that the flow around the street canyon has negligible effect on the core flow region. Symmetric boundary condition is employed at the top of the computation domain, that is, the velocity along the normal direction of the boundary is zero, and the gradient of all physical quantities is zero. This setting is the same as the centerline in the confined space and the top boundary of the semi-confined space.

When the fluid flows through a wall surface with temperature difference, heat transfer takes place and a temperature gradient is formed in the flow near the wall. The temperature of the fluid far from the wall surface is uniform. Therefore, it can be assumed that all the heat transfer process happens in the fluid layer with a temperature gradient, which is the thermal boundary layer. Similar to the flow pattern in the entrance length between the two parallel plates, the fluid flow is also divided into the free flow and the boundary layer flow (Fig. 1b) based on temperature profile. Therefore, theories applicable to the flow in the entrance region of confined spaces should also work for the boundary layer of semi-confined spaces, for example, the field synergy theory (Guo et al., 1998). Similarly, the concentration boundary layer occurs when there is a concentration difference between the fluid and the wall surface (Fig. 1c). Due to the similarity between convective heat transfer and convective mass transfer, many research theories used to study heat transfer are also applicable to convective mass transfer.

3. Field synergy theory

Guo et al. (1998) compared the two-dimensional flat laminar boundary layer problem to the heat conduction between two parallel flat plates with an internal heat source. According to the heat transfer laws of the two processes, the corresponding energy conservation equations can be obtained as follows:

$$\rho c_p\left(u\frac{\partial T}{\partial x}+v\frac{\partial T}{\partial y}\right)=\frac{\partial}{\partial y}\left(\lambda\frac{\partial T}{\partial y}\right) \tag{1a}$$

The energy conservation equation for heat conduction (ignoring heat conduction in the x-direction) is as follows:

$$-q(x,y)=\frac{\partial}{\partial y}\left(\lambda\frac{\partial T}{\partial y}\right) \tag{1b}$$

where λ is the thermal conductivity of the fluid medium, ρ is the density, c_p is the specific heat capacity, and q is the intensity of the internal heat source, i.e., the heat generated per unit time and unit volume.

The above two equations are respectively integrated in the boundary layer and two parallel plates:

$$\int_0^{\delta_{t,x}}\rho c_p\left(u\frac{\partial T}{\partial x}+v\frac{\partial T}{\partial y}\right)\mathrm{d}y=-\lambda\frac{\partial T}{\partial y}|_w=q_w(x) \tag{2a}$$

$$\int_0^{\delta_{t,x}}\overline{q}(x,y)=-\lambda\frac{\partial T}{\partial y}|_w=q_w(x) \tag{2b}$$

where $\delta_{t,x}$ is the thickness of the thermal boundary layer at x. The right sides of Eqs. (2a) and (2b) are the wall heat flow at x, the left side of Eq. (2a) is the sum of the convective heat source terms in the boundary layer at x, and the left side of Eq. (2b) is the sum of the heat sources at the section between the two plates at x. It is clear that the greater the sum of the heat sources, the greater the wall surface heat flow there, which is the concept of source strengthening. To further analyze the enhancement of convective heat transfer, the convection term on the left side of Eq. (2a) is rewritten into a vector form:

$$\int_0^{\delta_{t,x}}\rho c_p\left(\vec{U}\cdot\nabla T\right)\mathrm{d}y=-\lambda\frac{\partial T}{\partial y}|_w=q_w(x) \tag{3}$$

where $\vec{U}$ is the velocity vector of the fluid. Dimensionless variables are then introduced as follows:

$$\overrightarrow{\overline{U}}=\frac{\vec{U}}{U_\infty},\nabla\overline{T}=\frac{\nabla T}{(T_\infty-T_w)/\delta_t},\overline{y}=\frac{y}{\delta_t},T_\infty>T_w \tag{4}$$

The dimensionless relationship can then be determined as:

$$\mathrm{Re}_x\mathrm{Pr}\int_0^1\left(\overrightarrow{\overline{U}}\cdot\nabla\overline{T}\right)d\overline{y}=Nu_x \tag{5}$$

$$\overrightarrow{\overline{U}}\cdot\nabla\overline{T}=\left|\overrightarrow{\overline{U}}\right|\cdot\left|\nabla\overline{T}\right|\cos\alpha \tag{6}$$

where α is the angle between fluid velocity vector and the temperature gradient, namely the field synergy angle.

Therefore, there are three ways to strengthen heat transfer: (1) increasing the Reynolds number, (2) increasing the Prandtl number, and (3) increasing the dimensionless integral value.

Since its proposition, the field synergy theory has been applied increasingly more often in the study of heat transfer enhancement (Zhou et al., 2006; Hamid et al., 2014; Yan et al., 2012; Jia et al., 2016). They fully explored the field synergy theory to guide enhanced heat transfer in all kinds of confined spaces.

Based on the analogy of the three transmission laws, Chen et al. (2008) extended the convective heat transfer field synergy principle to the field of convective mass transfer. According to the concentration conservation equation of the steady-state mass diffusion of the three-dimensional passive term, they integrated the equation in the entire diffusion domain, and then used Gauss's theorem to convert the volume integral into a surface integral. On a surface where mass diffusion does not occur, the concentration gradient is zero, as is the integral value. Additionally, the inlet and outlet wind speeds are very large, and the concentration gradient is small and can be ignored. The final equation is simplified as:

$$\int_\Omega|U||\nabla C|\cos\beta dV=\int_S\vec{n}(\rho D\nabla C)dS \tag{7}$$

where ρ is the air density (kg/m^3), U is the fluid velocity (m/s); ∇C is the component concentration gradient, D is the mass transfer diffusion coefficient (m^2/s), and β is the angle between the velocity vector and the component concentration gradient vector. The dimensionless velocity and concentration gradient are respectively defined as:

$$\overline{U}=\frac{\overrightarrow{U}}{\sqrt{U_x^2+U_y^2}} \tag{8}$$

$$\overline{\nabla C}=\frac{\overrightarrow{\nabla C}}{\sqrt{\nabla C_x^2+\nabla C_y^2}} \tag{9}$$

The dimensionless variables are substituted into Eq. (7), and the equation is deformed to obtain the Sherwood number, S_h, which characterizes the relative sizes of convective mass transfer and diffusion mass transfer. The diffusion of pollutants in the street canyons is mainly affected by the ambient wind in the form of convective mass transfer between the airflow and the surface of street canyons and turbulent motions (Michioka et al., 2011). Therefore, it is considered that the Sherwood number can be used to measure the effectiveness of pollutant dispersal in street canyons. The Sherwood number is expressed as follows:

$$Sh=\mathrm{Re}Sc\frac{\int_\Omega\overline{U}\cdot\overline{\nabla C}dV}{V} \tag{10}$$

where $Sh=\frac{h_m d}{D}$, h_m is the convective mass transfer coefficient, and the Schmidt number, $Sc=\frac{\nu}{D}$, is the ratio of kinematic viscosity coefficient to mass diffusion coefficient. The dynamic viscosity coefficient ν of the air is 14.8×10^{-6} m^2/s. The diffusion coefficient of the gaseous pollutant D in the air is 2.88×10^{-5} m^2/s. Hence, $S_c=0.514$.

From the analysis of Eq. (10), it is clear that the size of the Sherwood number is not only related to the sizes of the Reynolds and Schmidt numbers, but also depends on the coordinate angle between the velocity vector and the concentration gradient vector, i.e., the integration value of the dot product of the two vectors in the target area. Therefore, this integral value that characterizes synergy is defined as the field synergy number, which physically represents the total dimensionless mass transfer intensity in the entire region:

$$Fc_m=\frac{\int_\Omega\overline{U}\cdot\overline{\nabla C}dV}{V} \tag{11}$$

The larger the dot product of the two vectors, the larger the field synergy number, the larger the Sherwood number, and the better the convective mass transfer effect. The expression of the field synergy angle is given as follows:

$$\beta=arccos\left(\frac{\overline{U}\cdot\overline{\nabla C}}{\left|\overline{U}\right|\left|\overline{\nabla C}\right|}\right) \tag{12}$$

Similarly, there are also three ways to enhance the convective mass transfer: (1) increasing the Reynolds number, (2) increasing the Schmidt number, and (3) increasing the value of the dimensionless integral number of field synergy, F_{cm}.

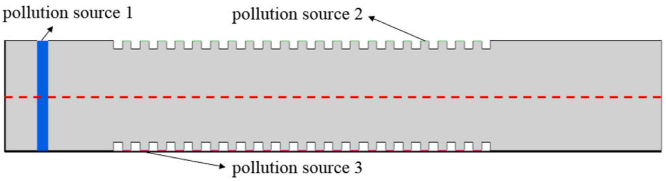

Fig. 2. The diagram of two infinitely long plates with grooves.

In addition, according to the improved field synergy theory, Wu et al. (2014) investigated a CO_2 capture process with a high capture rate and low energy consumption. Wang and Dai (2018) studied the spray effects of different geometric rod groups and different operating modes in a spray tower, and analyzed the methods by which to improve the mass transfer effect of the spray tower using field synergy theory. Similarly, field synergy theory can also be applied to enhance mass transfer in a restricted space. Therefore, whether the field synergy theory is applicable to the spread of pollutants in the open space like urban street canyons is worthy of investigation.

4. Verify the applicability of field synergy theory in street canyons

By comparing the pollution dispersion of the ambient wind passing over the urban street canyons and the convective heat transfer of the fluid flowing through two parallel plates, similarities are observed between the two processes. First of all, the ambient wind passing through the urban street canyons forms a layer with a large temperature and concentration gradient at the bottom of the flow, i.e., the thermal or concentration boundary layer. In the free flow above the boundary layer, temperature and pollutant concentration are basically unchanged. This is similar to the flow in the entrance region to a confined space, where the flow divides into the core flow and boundary layer flow. Secondly, in the flow entrance region to a confined space, the flow in the boundary layer does not affect the core flow. Hence, the flow can be regarded as symmetric about the centerline. As mentioned above, in the numerical simulation study of street canyon pollution, the top boundary condition of the computational domain is also set to symmetry, which is consistent with the centerline in the confined space and the top of the semi-confined space. Last but not least, through the above analogy between the characteristics of convective heat transfer and those of convective mass transfer, established research theories for studying heat transfer are also applicable to convective mass transfer. Due to the similarities in geometric boundary conditions and flow patterns, we can take advantage of field synergy theory applications in confined space to guide the study of pollution dispersion in urban street canyons.

To prove that the field synergy theory can be applied in street canyon models, the diffusion of pollutants between two infinitely long plates with grooves is investigated from the aspect of convection mass transfer in confined spaces. The geometric model for two infinitely long plates can be simplified to two dimensions, as illustrated in Fig. 2. The geometric dimensions of the two models were set as follows: the distance between the two plates was 5 mm, and the length of the plates was 30 mm. A CO belt pollution source of $x \times y = 0.5$ mm $\times$ 5 mm was set at 1.5 mm from the entrance (the blue areas in Fig. 2). A pollution source with 0.5 mm in length and 0.1 mm in width is set between each two grooves with an intensity of 10^{-5} (kg/(m^3·s), namely, the pollution source 2 (the green area of the upper plate in Fig. 2) and the pollution source 3 (the red area of the lower plate in Fig. 2). The height of the groove in Fig. 2 was 0.5 mm. The boundary conditions of the model were set as follows: the entrance at the left was set as the velocity inlet, and the given uniform wind speed was 0.05 m/s. The right exit was set to outflow conditions. The upper and lower walls were set to no-slip boundary conditions. Because the two models are completely symmetrical about the symmetry plane represented by the red dotted line, a half-model can be used for research to save computing resources. For the half-model, the boundary condition at the red dotted line was set as a symmetry condition, and the other parts remained unchanged.

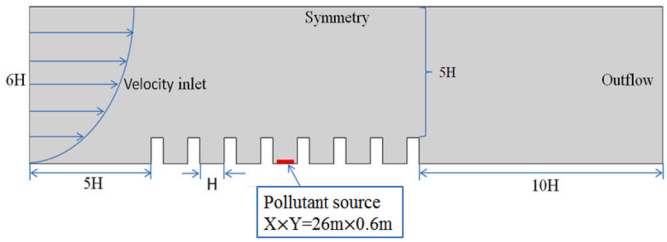

Fig. 3. Geometric model and boundary conditions.

To validate whether the half-model can replace the full model, the CO concentration profiles of the full model and the half-model of the two plates were compared. As shown in Fig. A1, the distribution of the CO mass fraction in the full model was found to be completely symmetric. The half-model of the structure was completely consistent with the contours of CO concentration in the corresponding area of the full model. To quantitatively analyze the calculation results of the two models, the CO concentration value and the velocity value along the x-axis on the reference line $y = 2$ mm were compared, and the results are shown in Fig. A2. The relevant physical quantities of the full and half-models of the two structures were found to almost coincide. This fully proves that, the half-model can replace the full model for related research on pollutant dispersion, hence, the half-model was adopted. Besides, for the comparison of the classic urban street canyon model (Fig. 3) with the half-model of two infinitely long flat plates with grooves, their geometric structures were similar and their boundary conditions were set to be the same. Therefore, we believe that the field synergy theory applied in confined space can also be used in the numerical simulation of pollution dispersion in urban street canyons.

5. Physical model and mathematical model

5.1. Physical model

The research in this paper is based on a classic multi-street canyon model. Research by Mei et al. (2019) revealed that for street canyons with the aspect ratios $H/W = 1$ (building height to street width) and $L/W > 20$ (building length to street width), two-dimensional simulation can replace three-dimensional simulation. This paper focuses on long canyons, so the two-dimensional simulation was applied. As shown in Fig. 3, the street canyon model was set with 7 continuous street canyons, the 4th of which was the target street canyon, and the building height was set to $H = 30$ m. The traffic road was located in the center of the street, and the total traffic lane was 26 m long. Two pavements located on both sides of the street were each set as 2 m wide. The roadway was provided with a uniform source of surface pollution with a width of 26 m and a height of 0.6 m. The calculated field was as follows: the entrance boundary was 5H from the first building, the velocity inlet was set in the form of gradient wind, the exit boundary was 10H from the 8th building, and the upper boundary was 5H away from the top of the building. Based on these criteria, the size of the entire computational domain was 780 m $\times$ 180 m.

5.2. Mathematical model

CFD approaches used in pollutant dispersion modelling mainly include large eddy simulation (LES) (Zhong et al., 2015, 2017; Hideki et al., 2018; Wang et al., 2018) and Reynolds-Averaged Navier-Stokes equations simulation (RANS) (Cui et al., 2017). Recently, Du et al. (2020) applied transport-based recurrence Computational Fluid Dynamics (rCFD) to simulate atmospheric pollutant dispersion around a

building. According to Keigo et al. (2018), compared with LES, the prediction of the k-ε model regarding the mean wind velocity and turbulent statistics in urban canyons is less accurate. However, LES may require sufficient computing resources and longer computing time. RANS method was widely used in near-field dispersion around buildings. Chan et al. (2002) compared different RANS characteristics of turbulence models, and it was found that the RNG k-ε model was the most optimum turbulence model coupled with the two-dimensional street canyon model. The RNG k-ε model is derived from the standard k-ε model using the statistical method of renormalization group theory. Moreover, this model performs well in the prediction of pollutant concentration according to Blocken et al. (2008). Therefore, to ensure calculation accuracy and save calculation resources, the RNG k-ε model was used to simulate the diffusion law of pollutants in urban street canyons.

In street canyons, the air velocity is low, and the air is considered to be an incompressible fluid. Thus, the flow of viscous incompressible fluids was described by the Navier-Stokes equation. It was assumed that the incoming wind and source intensities did not change with time. The corresponding continuity equation, momentum equation, energy equation, component transport equation, and RNG k-ε equation are as follows.

The continuity equation:

$$\frac{\partial u_i}{\partial x_i} = 0 \tag{13}$$

The Navier-Stokes equation:

$$\frac{\partial}{\partial t}(\rho u_i) + \frac{\partial}{\partial x_j}(\rho u_i u_j) = -\frac{\partial p}{\partial x_i} + \frac{\partial \tau_{ij}}{\partial x_j} + \rho g_i + F_i \tag{14}$$

$$\tau_{ij} = \left[\mu\left(\frac{\partial u_i}{\partial x_j} + \frac{\partial u_j}{\partial x_i}\right)\right] - \frac{2}{3}\mu\frac{\partial u_i}{\partial x_i}\delta_{ij} \tag{15}$$

The energy equation:

$$\frac{\partial}{\partial t}(\rho E) + \nabla\cdot(\vec{\nu}(\rho E + p)) = \nabla\cdot\left(k_{eff}\nabla T - \sum h_j \overline{J}_j + \left(\overline{\overline{\tau}}_{eff}\cdot\vec{\nu}\right)\right) + S_h \tag{16}$$

where k_{eff} is the effective thermal conductivity ($k + k_f$, k_f is the thermal conductivity caused by the turbulence as determined by the turbulence model), and $\overline{J}_j$ is the component's diffusion flux. The first three terms on the right side of Eq. (16) represent the energy transfer due to heat conduction, component diffusion, and viscous dissipation, respectively. S_h includes exothermic (endothermic) heat and any other user-defined volumetric heat source.

The component transport equation is as follows:

$$\frac{\partial C_i}{\partial t} + u_j\frac{\partial C_i}{\partial x_j} = \frac{1}{\rho}\frac{\partial}{\partial x_j}\left[\left(D + \frac{\mu_t}{Sc_t}\right)\frac{\partial C_i}{\partial x_j}\right] \tag{17}$$

The RNG k-ε equation:

$$\frac{\partial}{\partial t}(\rho k) + \frac{\partial}{\partial x_i}(\rho k u_i) = \frac{\partial}{\partial x_j}\left(\alpha_k \mu_{eff}\frac{\partial k}{\partial x_j}\right) + G_k + G_b - \rho\varepsilon - Y_M + S_k \tag{18}$$

$$\begin{aligned}\frac{\partial}{\partial t}(\rho\varepsilon) + \frac{\partial}{\partial x_i}(\rho\varepsilon u_i) = {} & \frac{\partial}{\partial x_j}\left(\alpha_\varepsilon \mu_{eff}\frac{\partial \varepsilon}{\partial x_j}\right) + C_{1\varepsilon}\frac{\varepsilon}{k}(G_k + C_{3\varepsilon}G_b) \\ & - \left[\rho C_{2\varepsilon} + \frac{C_\mu \rho \eta^3(1-\eta/\eta_0)}{1+\beta\eta^3}\right]\frac{\varepsilon^2}{k} + S_\varepsilon\end{aligned} \tag{19}$$

where α_k and α_ε are the k and ε values of the inverse effective Prandtl number, μ_{eff} is the effective turbulent viscosity, $\eta = Sk/\varepsilon$, S is the deformation tensor, $C_{1\varepsilon} = 1.42$, $C_{2\varepsilon} = 1.68$, $C_\mu = 0.0845$, and generally $\beta = 0.012$ and $\eta_0 = 4.38$.

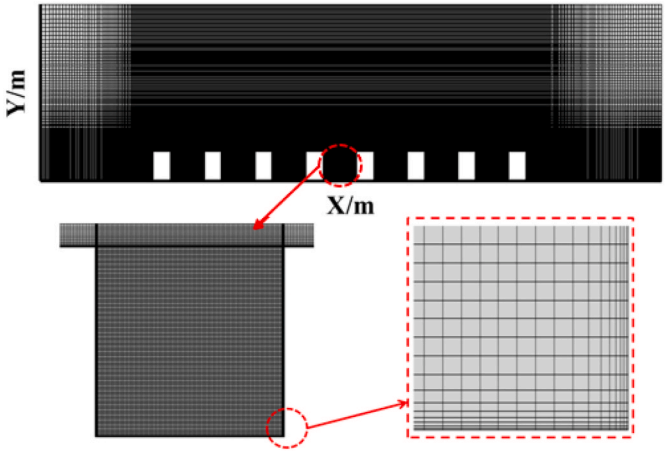

Fig. 4. Schematic diagram of the mesh demarcation.

5.3. Meshing skills and sensitivity analysis

The entire calculation domain uses structured meshes. To ensure the applicability of standard wall functions, eight-layer boundary layer grids were set up on the ground and the walls of the building. The first layer was set to 0.02 m to ensure that the dimensionless wall distance $y+$ of the first-layer mesh met the calculation requirements. For the target street canyon, the grid size of $\Delta x \times \Delta y = 0.2$ m $\times$ 0.2 m was used, and $\Delta x \times \Delta y = 0.5$ m $\times$ 0.2 m was used for other street canyons. The expansion ratio of mesh in the y-direction and outside the street canyon in the x-direction was less than 1.03 to stabilize the numerical oscillation, accelerate the convergence, and improve the computational efficiency. Fig. 4 presents a schematic diagram of the mesh demarcation.

The general CFD commercial software ANSYS FLUENT 15.0 was used for calculation. The SIMPLE algorithm was then used to compile the stream through user-defined function methods. The discretization methods of both convection and diffusion terms were selected in the Green-Gauss cell based and second-order upwind scheme, and the standard algorithm was used for pressure interpolation. The convergence factor of the energy equation was set to 1×10^{-8}, and the convergence factors of other variables were set to 1×10^{-5}. The iterations were continued until the relative error in the conservation equation was less than 1×10^{-5} and that in the energy equation was less than 1×10^{-8}.

To guarantee the calculation accuracy, the independence of the mesh was verified. Three mesh numbers, namely 207840, 249272, and 306764, were selected and carried out with the same machine under the same operating conditions, namely the reference wind speed of 2 m/s and the pollution source intensity of 10^{-7} kg/(m^3·s). In the target street canyon, a straight line (where $y = 15$ m, x is from 300 m to 330 m) was selected to compare the speed profiles and the mass fraction of CO under the three mesh conditions. Fig. 5 shows very similar calculation results. The error was the greatest when the number of grids was 207840. The calculation results of the other two grids were almost identical. These results demonstrate that further increasing the number of grids will not cause significant changes in the calculation results. Therefore, the number of meshes of 249272 was selected as the basic mesh system in this study.

5.4. Boundary conditions

Velocity-inlet was applied in the inlet boundary. The wind velocity profile in this 2D model is described by an exponential law (Wang and Chen, 2012):

$$U_z = U_{ref}\left(\frac{z}{z_{ref}}\right)^{\alpha} \tag{20}$$

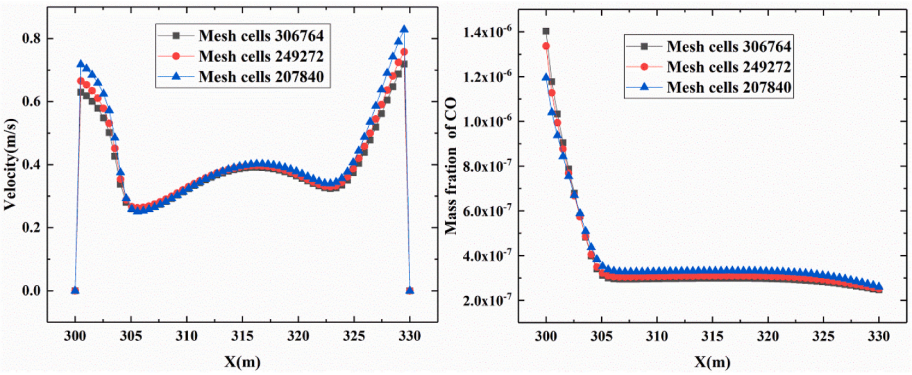

Fig. 5. Grid independence test results.

$$k = \frac{(U^*)^2}{\sqrt{C_\mu}} \tag{21}$$

$$\varepsilon = \frac{(U^*)^3}{kz} \tag{22}$$

where U_{ref} indicates the speed at the reference altitude Z_{ref}, and the reference height in this paper was 30 m. Additionally, α is the ground roughness index, which was taken as 0.2, U^* represents friction velocity, k is the von-Karman constant, which was taken as 0.42, and $C_\mu = 0.09$.

The upper boundary of the computational domain was set to symmetry conditions, which is a zero-gradient boundary. On the ground and the walls of the buildings, the standard wall function was introduced for near-wall correction. No-slip wall boundary conditions were applied to all wall surfaces.

5.5. The dimensionless pollution concentration and the volumetric average pollution concentration

Pollution in street canyons can be categorized into gaseous pollutants and solid particles. Compared with gaseous pollutants, the diffusion effect of particulate matter is not only affected by wind speed, thermal buoyancy, etc., but is also closely related to the particle size of the particulate matter and the deposition effect caused by different amounts of air humidity. To simplify the analysis, CO, which accounts for a relatively large part of vehicle exhaust gas and has stable chemical properties, was selected as the tracer pollutant to study its diffusion law. For comparison and analysis, the pollutant concentration was normalized by the following equation:

$$K = \frac{\rho_{air} C U_{ref} H}{S_e A_c} \tag{23}$$

where C represents the mass fraction of the pollutants obtained from the FLUENT simulation, U_{ref} is the wind speed at the reference altitude (m/s), H is the building height, S_e is the total emission intensity of the pollutant source (kg/(m^3·s)), and A_c is the control area of the pollution source in the present simulation (m^2). The concentration of pollutants was normalized to effectively avoid the influences of factors such as source intensity and street geometry on the calculation results.

The calculation formula of the average pollutant concentration in the street canyon is as follows:

$$\overline{C} = \frac{\int_\Omega C_i dS}{S_\Omega} \tag{24}$$

where C_i is the averaged mass fraction in cell i, Ω represents the target street canyon computational domain, and S_Ω represents the target street canyon control area.

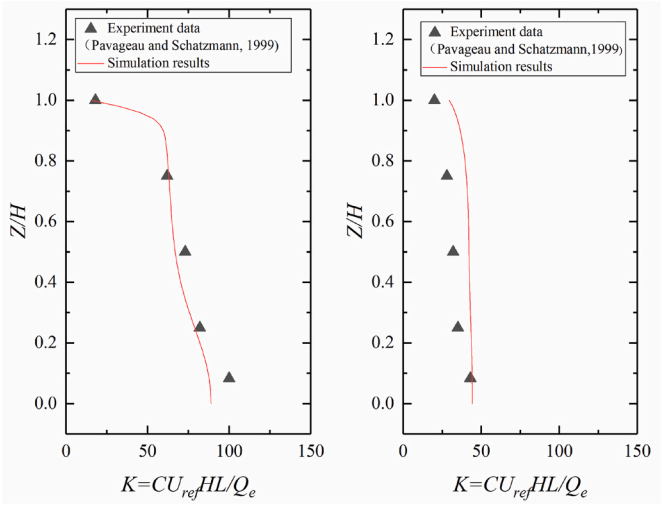

Fig. 6. Comparison of the normalized concentration in the vertical direction obtained from simulations and experiments.

5.6. Model validation

Model validation is an important procedure to ensure the accuracy and reliability of numerical simulation results. In order to increase reliability, two experimental validations were performed. The applicability of the geometric model was validated through wind speed profiles in the first validation. The second validation is the reliability of simulated pollutant concentrations.

In the first validation, the data used in the present study to evaluate the CFD model were obtained from Michioka et al. (2011). Wind tunnel experiments were conducted at the Japan Central Electric Power Research Institute. The size of the experimental wind tunnel was 17 m × 3 m × 1.7m. Seven Irwin-type vortex generators were arranged at the test entrance at $z = 0.65$ m, and 3 L-shaped partitions were arranged at equal intervals on the ground at the entrance from 0 m to 5 m. To produce near-surface turbulent flow, 28 identical cubes (1.56 m × 0.12 m × 0.12m) were laid at a distance of 10.5 m from the inlet with an equal spacing of 0.12 m (H) to simulate multiple street canyons. A gradient wind was set at the entrance boundary, the reference wind speed at $z = 2H$ was 1.15 m/s, and the 25th street canyon was used as the test street canyon. For the target street canyon, the wind speed changes along the z-direction were measured at three lines (where $y/H = 0$, $x/H = 0.25, 0.5, 0.75$) using a laser Doppler velocimeter.

In the second validation, the concentrations obtained by RANS are compared with those in the experiments conducted by Pavageau and

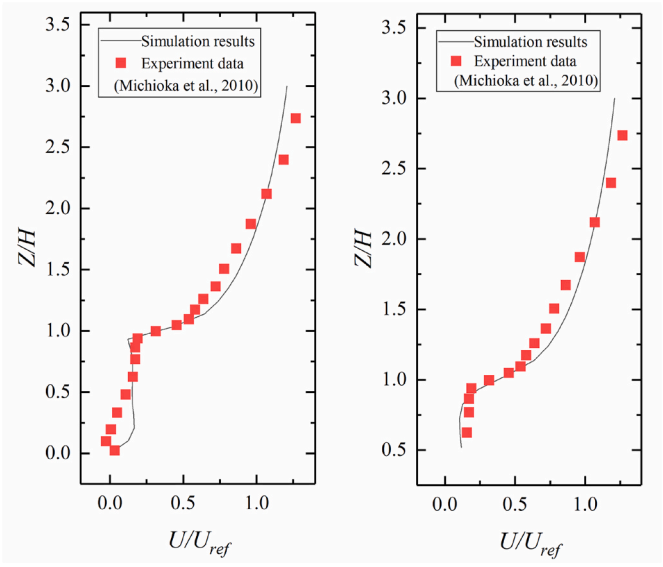

Fig. 7. Comparison of the normalized velocity in the vertical direction obtained from simulations and experiments.

Schatzmann (1999). The pollutant emission rate Q is represented by a ground-level continuous pollutant line source of length Ly placed parallel to the spanwise axis from $x/H = 0.0$ to $x/H = 1.0$. The tracer gas ethane, which is used in this wind-tunnel experiment and our corresponding numerical simulation verification, is only emitted from a line source within the canyon. As shown in x axis of Fig. 6, the normalized concentration K is normalized by U_{ref} (the free-stream velocity, 1 m/s) taken at 650 mm above the floor in the free-stream region of the flow above the test street. C is the actual measured concentration, H is the block height (0.06 m), L is the length of the line source, and Q_e is the total emission.

According to the two experiments, the same geometric models were established, and consistent boundary conditions were set. The calculation results are presented in Figs. 6 and 7. The simulation data was found to agree well with the experimental data. The average deviation between the simulation results and the measured results was less than 10%. However, when $x/H = 0.25$, $z/H < 0.4$, the simulated values are slightly higher than the experimental values. This may be due to the insufficient accuracy of the RANS model in the simulation of the near-wall surface at the bottom of the street canyon. As to the concentration, Fig. 6 shows that the numerical simulation results of normalized mean concentration at $x/H = 0.0$ agree well with the experiment data. However, there is a small deviation in the normalized mean concentration at $x/H = 1.0$, which may be due to the difference in the airflow generated by the vortex generator and the simulation. Despite some slight differences, the RNG k-ε turbulence model is feasible for solving fluid flow and pollutant dispersion.

6. Application of the field synergy theory to the analysis of pollutant dispersion in street canyons

6.1. Impacts of the height of the viaduct and ambient wind speed in the street canyon

The construction of viaducts has become a powerful measure to alleviate the problems associated with dense buildings and heavy traffic in cities. However, the construction of urban viaducts has a great impact on the spread of pollutants in street canyons. Studying the effects of viaducts on the spread of pollutants in street canyons is critical to improving the air quality in street canyons and the living environment of residents in buildings near roads. The pollution of viaducts at 6 different heights (Hviaduct = 0.5H, 0.6H, 0.7H, 0.8H, 0.9H, 1.0H) and with a bridge width of 20 m in a symmetrical street canyon with an aspect ratio of 1 was investigated. The field synergy theory was used to quantitatively analyze the intrinsic relationship between pollutant migration and convective mass transfer in street canyons.

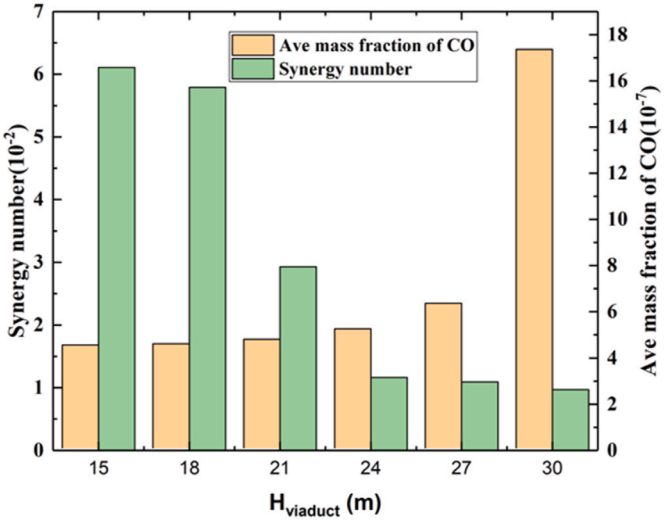

Fig. 8. Influences of the viaduct height on the pollution dispersion in street canyons.

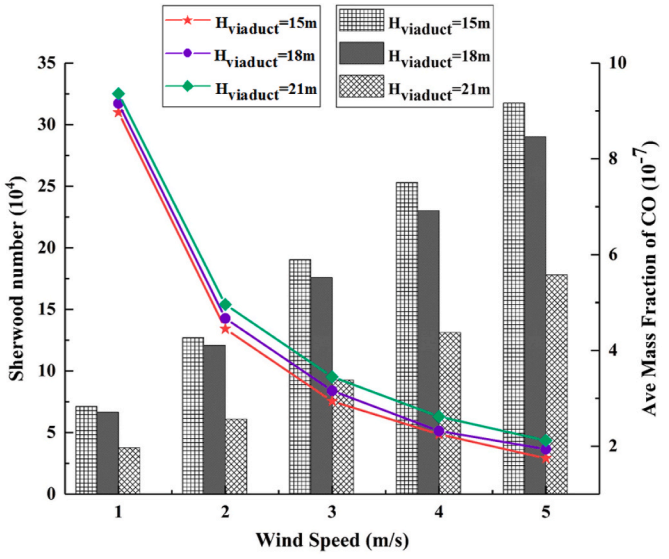

Fig. 9. Influences of the ambient wind speed on S_h (the bar chart) and the average pollution concentration (the dot plot) in street canyons.

Fig. 8 presents the relationship between the field synergy number (F_{cm}) and the average concentration in the target street canyon for the six cases. The results show that as the height of the viaduct increased, the field synergy number gradually decreased, indicating that the synergy between the velocity field and the concentration gradient field in the street canyon worsened. When the other conditions remained the same, the convective mass diffusion effect became poor. For street canyons with an aspect ratio of 1, when the viaduct height was equal to the street canyon depth, the field synergy number was the smallest, and the average concentration of pollutants in the street canyon was more than double that in other cases. Therefore, when constructing a viaduct, the erection height of the viaduct should not be the same as its depth in the

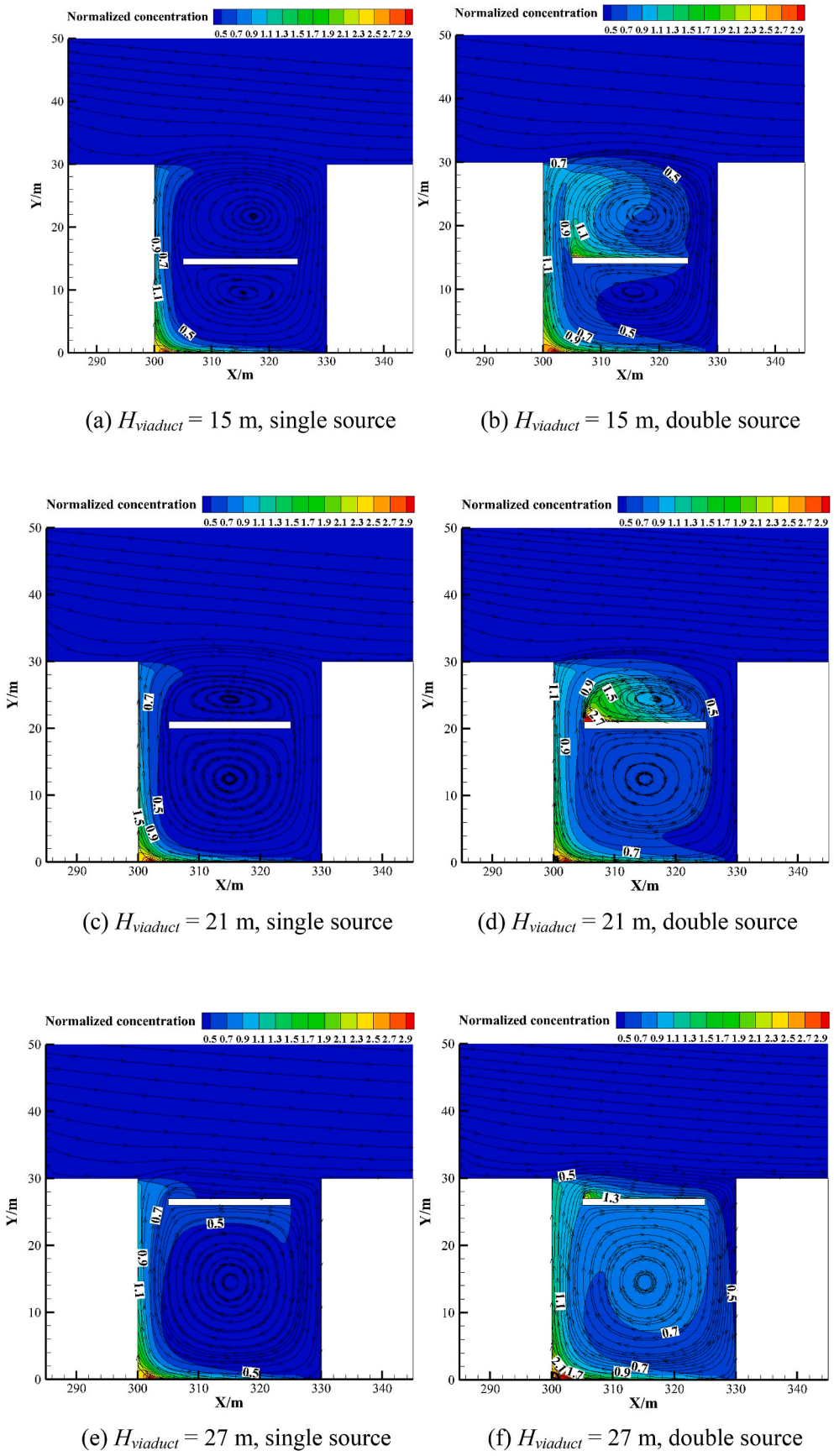

Fig. 10. Normalized concentration distributions and streamline diagram in a street canyon with three different viaduct heights. In each case, two pollution source settings (single and double sources) are investigated.

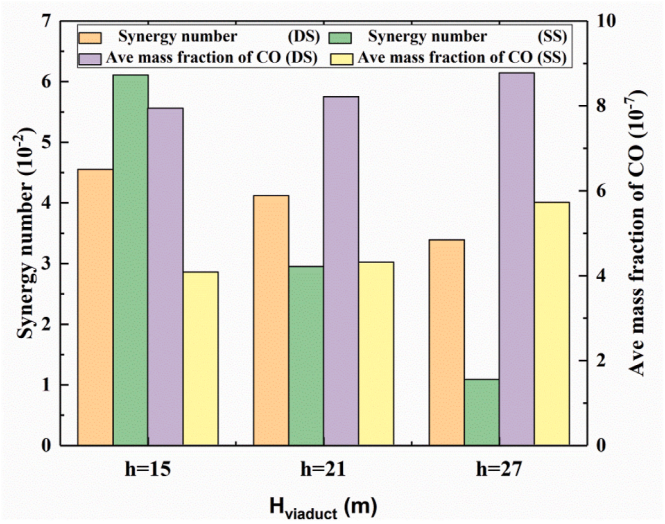

Fig. 11. Histograms of field synergy numbers and average concentrations of three viaducts under different pollution sources (SS: single source; DS: double source).

street canyon. Fig. 9 shows the impact of ambient wind speed on the Sherwood number (S_h) and the average pollution concentration of the street canyon under the conditions of three viaduct heights. With the increase of the wind speed, the speed of the airflow in the street canyon increased, the modulus of the velocity vector increased, and the Reynolds number increased. It is necessary to use the Sherwood number to characterize the effect of convective mass transfer. For the same street canyon geometry, the synergy between the concentration gradient and the velocity vector changed little. Thus, the key to enhancing the effect of convective mass transfer is the increase in velocity. As the Sherwood number increased, the average concentration in the street canyon gradually decreased. It was also observed that the lower the viaduct construction height, the larger the Sherwood number, the better the convective mass transfer effect, and the smaller the average concentration in the street canyon.

6.2. Impact of pollution sources on viaducts in street canyons

After the viaduct is put into operation, pollutants emitted by motor vehicles on the bridge are a non-negligible source of pollution. The viaduct structure and the pollution source above it demonstrates a strong influence to the vortex structure and pollutant distribution in the street canyon, compared with street canyons without viaducts (Fig. A3). Because there are few pedestrians on the viaduct, a surface pollution source with the same width as the viaduct was installed on the viaduct ($x \times y = 20$ m $\times$ 0.6 m), and the pollution source intensity was the same as that on the ground, namely10^{-7} kg/(m^3·s); therefore, the influence of the pollution source on the bridge on the spread of pollutants in the street canyon can be compared.

Fig. 10(b) and (d), and 10(f) represent pollution sources set both on the viaduct and on the ground, while Fig. 10(a), (c), and 10(e), represent pollution sources set only on the ground. For the three single-source cases, the viaduct height settings were found to result in similar distribution characteristics of the pollutants in the street canyon. With the increase of the viaduct height, the area where pollutants spread gradually increased, extending toward the center of the street canyon. When pollution sources were also set up on the viaduct, the distribution characteristics of the pollutants at the three-level viaducts changed significantly. For the viaducts with the heights of 15 m and 21 m, two areas with high concentrations of pollutants appeared in the street canyon, including the leeward ground and the upper leeward side of the viaduct. When $H_{viaduct} = 27$ m, the pollutants in the upper part of the viaduct were more easily blown out of the street canyon by the incoming wind due to the clockwise vortex and the resistance of the viaduct surface. Therefore, the concentration of pollutants in the upper part of the viaduct was lower than that in the first two cases. Additionally, the pollutants in the street canyon were more uniformly distributed, and the pollutants on the leeward side were diffused. Compared with the first two cases, the environmental quality on the windward side deteriorated slightly.

Fig. 11 presents the average concentrations and field synergy numbers in the street canyon for three different heights of the viaduct. Fig. 12 demonstrates the contours of field synergy angle between the velocity and concentration gradient in the target street canyon for 6 cases. It can be determined that the distribution of the synergy angle was center-symmetrical with respect to the center of the vortex. For the setting of a single pollution source, as the height of the viaduct increased, the area with large synergy angle in the street canyon increased, and the average synergy angle increased, and the smaller the synergy number (the green bars in the histograms) in the target street canyon, the more unfavorable the diffusion of pollutants in the street canyon. This also corresponds to a larger average concentration of pollutants (the yellow bars in the histograms). It is worth noting that when the pollution source was set above the viaduct and the ground, with the change of height, the synergy situation of the field in the street canyon did not change significantly. Therefore, when pollution sources are set above the viaduct and the ground, the effect of the height of the viaducts on the diffusion of pollutants in the street canyon is less than that for a single pollution source. It was found that, for viaducts of the same height, different pollution source settings have different effects on field synergy. For $H_{viaduct} = 15$ m, when a pollution source was set on the viaduct, the area with a large synergy angle in the upper part of the viaduct became slightly larger, which worsened the overall synergy. However, when $H_{viaduct} = 21$ and 27 m, when a pollution source was set on the viaduct, the synergy angle of the upper area of the viaduct decreased, which promoted the field synergy of two vectors in the street canyon, and the field synergy number in the street canyon increased. This also explains why the difference in the average concentration decreased for the viaducts of three different heights when both sources of pollution were set.

6.3. Impact of roof shapes on pollution dispersion in street canyons

Building roofs in cities have different shapes. In order to study the influence of different roofs on the diffusion of pollutants in the street canyons, this work selects four typical roofs of flat roofs, double pitched roofs, upward pitched roofs, and downward pitched roofs for numerical simulation. According to the literature (Ding et al., 2019; Huang et al., 2015), the roof height is taken as 1/3 of the building height. The target street canyon is set to 4 adjacent consecutive street canyons, which are street canyon A, B, C, and D along the incoming flow direction. The boundary conditions are set the same as the numerical simulation above. To control the unique variable of the roof shape, the other physical conditions of each street canyon are set the same, as shown in Fig. 13.

It can be seen from the streamline diagram that the shape of the roof has a significant impact on the flow field in the street canyon. For flat roofs and downward pitched roofs, there is a clockwise vortex in the street canyon. For double pitched roofs and upward pitched roofs, two vortices in opposite directions, the lower vortex is counterclockwise and the upper vortex is clockwise. The upper vortex range of the double pitched roof is relatively large. The flow pattern in the street canyon determines the distribution characteristics of the pollutants in the street canyon. As shown in Fig. 14, for the flat roof and the downward pitched roof, the pollutants mainly gather on the leeward side of the street canyon. On the contrary, for the double pitched roof and the upward pitched roof, pollutants mainly gather on the windward side of the street canyon. According to the contour of the distribution of normalized concentration, it can be found that the double pitched roof and the

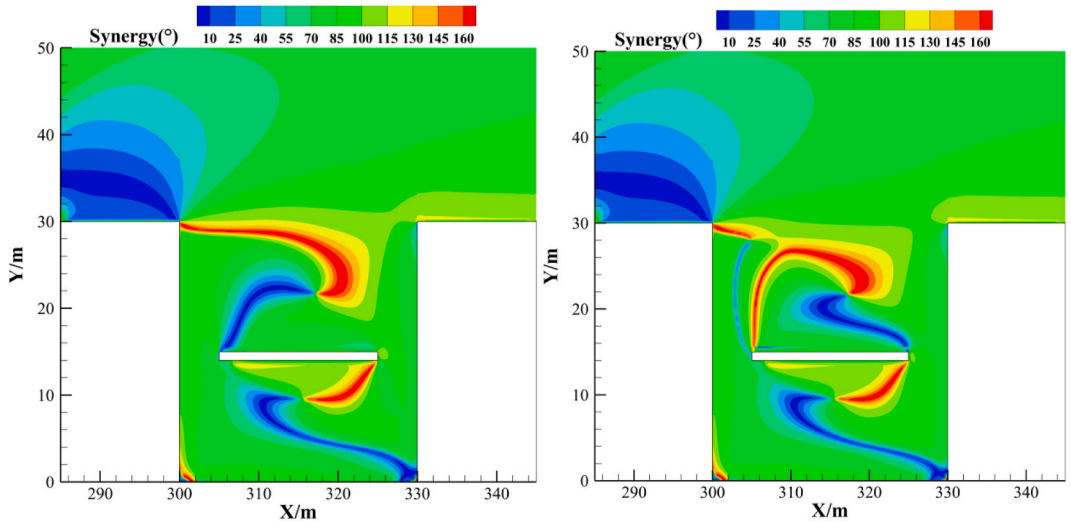

(a) $H_{viaduct}$ = 15 m, single source (b) $H_{viaduct}$ = 15 m, double source

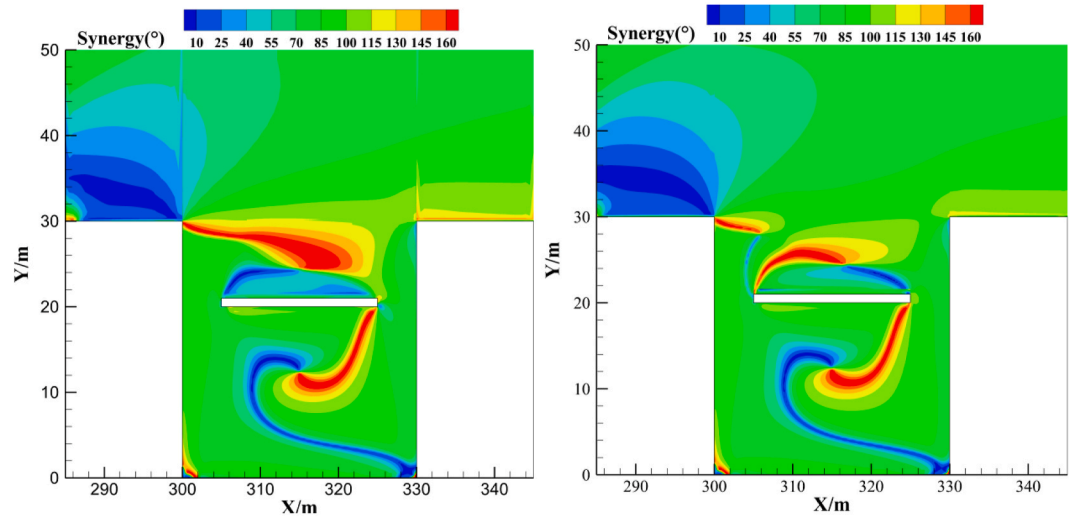

(c) $H_{viaduct}$ = 21 m, single source (d) $H_{viaduct}$ = 21 m, double source

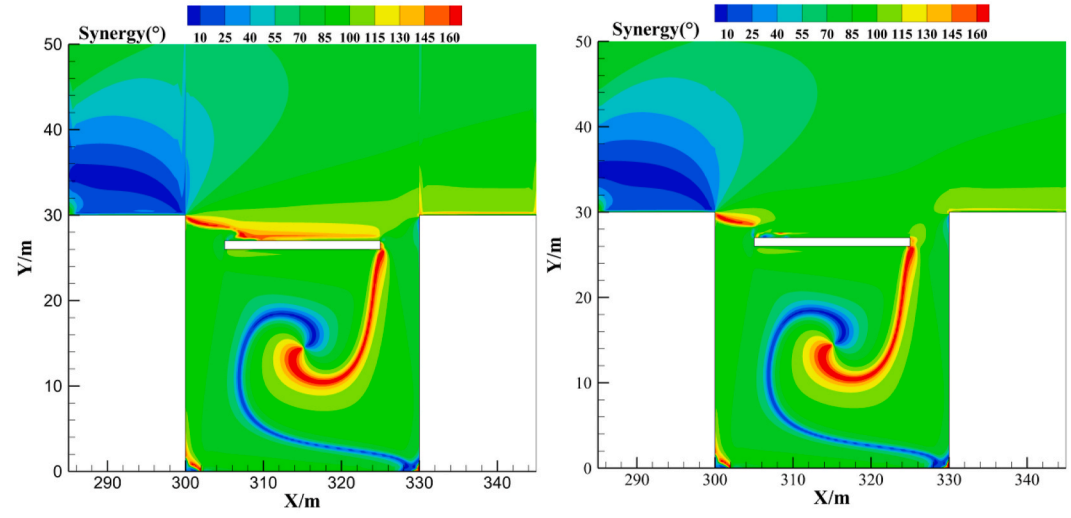

(e) $H_{viaduct}$ = 27 m, single source (f) $H_{viaduct}$ = 27 m, double source

Fig. 12. Synergy angle distributions of three types of viaducts under different pollution source settings.

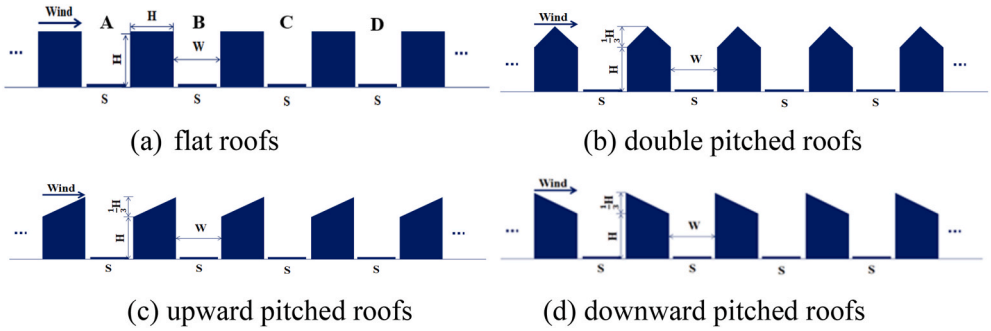

Fig. 13. Sketch of the urban street canyon configurations.

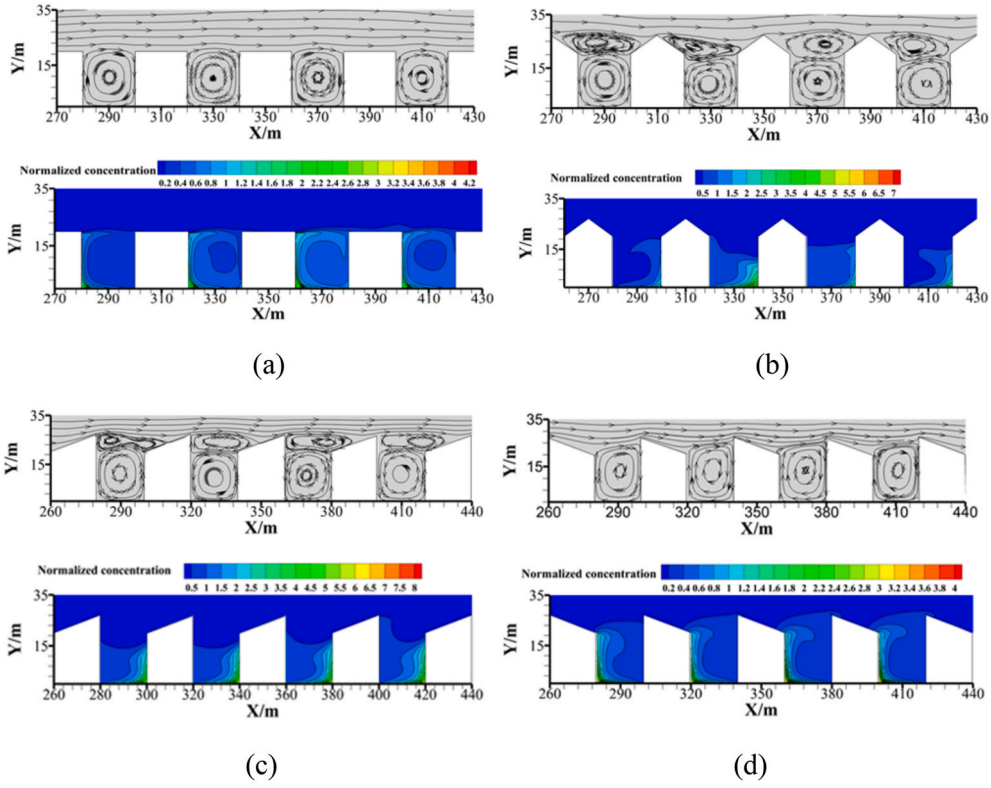

Fig. 14. Flow field diagram and concentration distribution in the street canyon with different roof shapes. (a) Flat roofs, (b) Double pitched roofs, (c) Upward pitched roofs, (d) Downward pitched roofs.

upward pitched roof have a large distribution area in the street canyon. This is because of the different vortex structures in the flow field of street canyons. Two vortices appear in the above two roof forms, which makes the pollutants entrained in a wider range, and the maximum pollutant concentration is much higher than the other two roofs, it is unfavorable for pedestrians and residents in the street canyon. It is also worth noting that the concentration of pollutants in the street canyons in the downwind direction does not increase regularly compared to the street canyons in the upwind direction. On the one hand, the spread of vehicle exhaust emissions in the street canyons is mainly limited to inside the street canyon. On the other hand, the setting of the concentration of pollution sources is relatively low, and the accumulation of pollutants in the air is not obvious.

In order to qualitatively analyze the influence of different roof shapes on the diffusion of pollutants in the street canyon, the Sherwood numbers that describing the mass transfer intensity were proposed according to the field synergy theory, and the results are shown in Fig. 15. The Sherwood numbers of flat roofs and downward pitched roofs are significantly higher than those of the other two roofs, indicating that these two roof shapes are beneficial to the diffusion of pollutants in the street canyon. For the double pitched roof, the Sherwood number can only reach 29%–78% of the flat roof; the situation of the upward pitched roof is even more unfavorable, and its Sherwood number can only reach 15%–31% of the flat roof. Moreover, the average concentration in each street canyon is also counted. As shown in Fig. 15, it can be found that the changing trend of the average concentration in each street canyon is exactly the opposite of the Sherwood number, which further proves the characterization effect of the Sherwood number. The smaller the Sherwood number, the worse the mass transfer and diffusion effect in the street canyon. Correspondingly, the higher the pollution level in the street canyon, the higher the average concentration. At this time, the average concentration in each street canyon of the upward pitched roof is 1.6–2.3 times that of the flat roof; the average concentration of each street canyon of the double pitched roof is 1.2–2 times that of the flat roof.

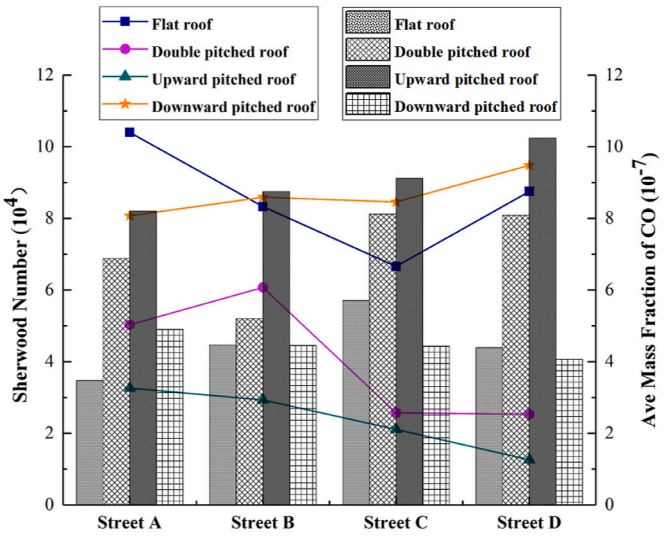

Fig. 15. The Sherwood number (the dot plot) and average concentration (the bar chart) in the street canyon with different roof shapes.

7. Discussion

In this paper, the similarities in geometric boundary conditions and flow patterns between the convective heat transfer model in a typical confined space and the convective mass transfer model caused by ambient wind passing over the street canyons were observed and reported. Based on the numerical results, the feasibility of applying field synergy theory in studying urban street canyons pollution was proved. On this basis, the field synergy theory was employed to analyze the effect of viaduct height, ambient wind speed, and various building roof shapes on the pollution dispersion in the street canyon. The extended field synergy theory can quantitatively analyze the influence of different factors on pollutant concentration, providing a new method for the study of vehicle exhaust pollution in the future.

As a preliminary study on the application of field synergy theory to the simulation of urban street canyons pollution, there are some limitations in our work. First of all, only the simple street canyons model was considered in the present work, lacking the analysis of complex street canyons with different aspect ratios and asymmetric configuration. Secondly, only the turbulence caused by ambient wind was considered whereas the turbulence induced by the movement of traffic flow in the street canyon was not sufficiently represented. Moreover, the influence of thermal-induced turbulence caused by solar radiation was not considered. Last but not least, the setting of pollution sources on the ground and above the viaduct is rather ideal, which may differ from the reality. The defects above need to be addressed by further work in the next stage.

8. Conclusions

Because of the similarity between physical processes of convective mass transfer and convective heat transfer, this study extended the field synergy theory governing the convective heat transfer process to the convective mass transfer of pollutant dispersion in urban street canyons. The field synergy theory was first extended from convective mass transfer in a small-scale (10^{-3}-10^{-1} m) confined space to a large-scale (10–10^3 m) opening space via both theoretical analysis and numerical verification in a confined space. Then the theory was applied to the assessment of pollutant diffusion in urban street canyons. The ambient wind speed, the settings of the viaduct and the shapes of the roof have been quantitatively evaluated. By comparing and analyzing the field synergy numbers, including Sherwood number, field synergy angle, the performance of pollutant dispersion in the street canyon was analyzed under different conditions quantitatively. The relationship between the Sherwood number and the pollutant dispersion in street canyons was revealed. The conclusions are summarized as follows.

(1) The convective mass transfer field synergy theory can be applied to the analysis of pollutant propagation laws in the semi-constrained space of urban street canyons. It provides new theoretical support for understanding the diffusion laws of pollutants in urban street canyons. Correspondingly, the Sherwood number (S_h) and the field synergy number (F_{cm}) provide new indexes for the quantitative evaluation of pollutant dispersion effects in street canyons.
(2) Based on the simulated results, the Sherwood number decreases with increased viaduct construction height and decreased wind speed, which is compatible with the observed growth of pollutant fraction in the street canyon. When the pollution source on the viaduct is considered, a less substantial influence of construction height on pollutant diffusion is observed and can be explained by the change of the field synergy angle, which further supports the application of field synergy theory for simulating street canyons.
(3) For the upward pitched roof, the Sherwood number can only reach 15%–31% of that for the flat roof; for the double pitched roof, the Sherwood number can reach 29%–78% of that for the flat roof. Consistent with the field synergy theory, the simulated average pollutant concentration in each street canyon with the upward pitched roof and the double pitched roof is 1.6–2.3 times and 1.2–2 times of that with the flat roof, respectively.

Credit author statement

Tingzhen Ming performed writing-original draft and conceptualization; **Tianhao Shi** and **Huina Han** performed wirting-original draft and theoretical analysis and part of numerical simulation; **Huina Han** performed wirting-original draft and part of numerical simulation; **Shurong Liu** performed writing-reference collection, literature review and data analysis; **Yongjia Wu** performed writing-editing and conceptualization; **Wenyu Li** performed writing-review and editing discussion; **Chong Peng** performed writing – review and conceptualization.

Declaration of competing interest

The authors declare that they have no known competing financial interests or personal relationships that could have appeared to influence the work reported in this paper.

Acknowledgement

This research was supported by the National Key Research and Development Plan (Key Special Project of Inter-governmental National Scientific and Technological Innovation Cooperation, Grant No. 2019YFE0197500), National Natural Science Foundation of China (Grant No. 51778511), the European Commission H2020 Marie S Curie Research and Innovation Staff Exchange (RISE) award (Grant No. 871998), Hubei Provincial Natural Science Foundation of China (Grant No.2018CFA029), Key Project of ESI Discipline Development of Wuhan University of Technology (Grant No. 2017001), National College Student Innovation and Entrepreneurship Training Program (Grant No. 20191049706008), and the Fundamental Research Funds for the Central Universities (Grant No. 2019IVB082). The authors of this article would like to express their sincere thanks to the three anonymous reviewers, for providing insightful comments and constructive advice that substantially improved the technicality of this article.

Appendix

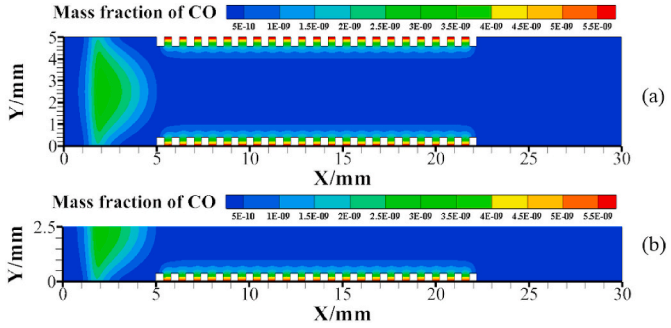

Fig. A1. Concentration distribution contours between two infinite plates with grooves: (a) full-model and (b) half-model.

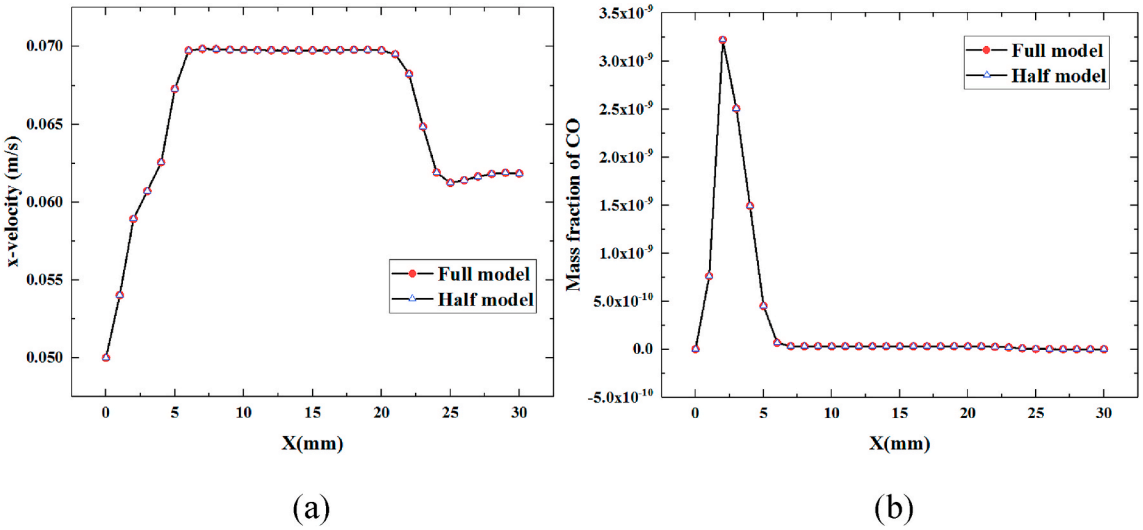

Fig. A2. Comparison between the full and half-models of two infinite plates with grooves: (a) x-velocity profiles; (b) mass fraction of CO.

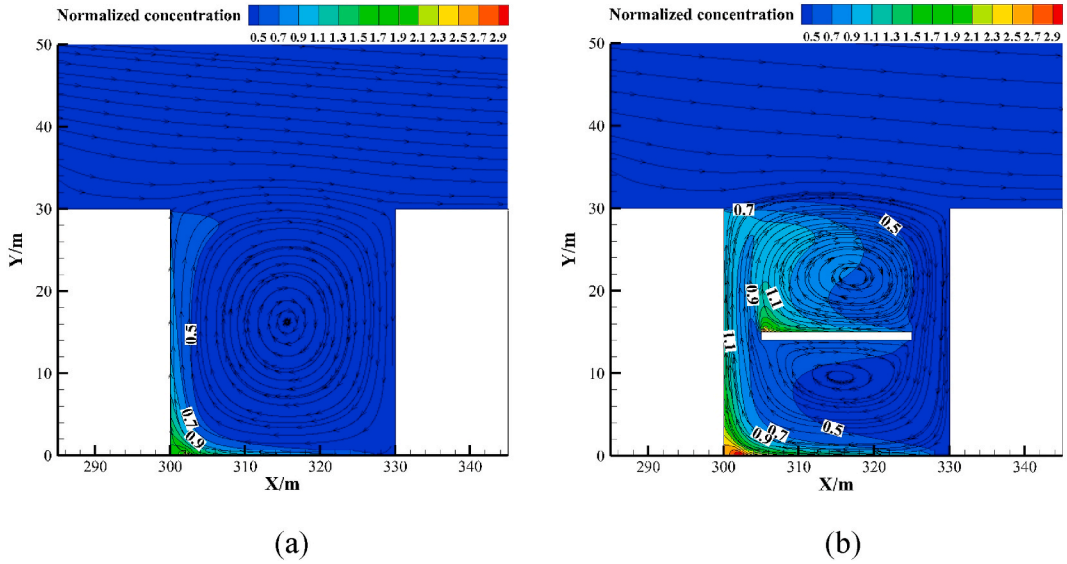

Fig. A3. Normalized concentration distributions of street canyon with: (a) no viaduct; (b) viaduct with a height of 15m.

References

Ahmad, K., Khare, M., Chaudhry, K., 2002. Model vehicle movement system in wind tunnels for exhaust dispersion studies under various urban street configurations. J. Wind Eng. Ind. Aerod. 90, 1051–1064.
Assimakopoulos, V.D., ApSimon, H., Moussiopoulos, N., 2003. A numerical study of atmospheric pollutant dispersion in different two-dimensional street canyon configurations. Atmos. Environ. 37, 4037–4049.
Bejan, Adrian. Convection Heat Transfer. 1984.
Baik, J., Kang, Y., Kim, J., 2006. Modeling reactive pollutant dispersion in an urban street canyon. Atmos. Environ. 41, 934–949.
Baratian, Z., Kaye, N.B., 2013. The effect of canyon aspect ratio on flushing of dense pollutants from an isolated street canyon. Sci. Total Environ. 443, 112–122.
Blocken, B., Stathopoulos, T., Saathoff, P., Wang, X., 2008. Numerical evaluation of pollutant dispersion in the built environment: comparisons between models and experiments. J. Wind Eng. Ind. Aerod. 96, 1817–1831.
Caton, F., Britter, R., Dalziel, S., 2003. Dispersion mechanisms in a street canyon. Atmos. Environ. 37, 693–702.
Chan, T., Dong, G., Leung, C., Cheung, C., Hung, W., 2002. Validation of a two-dimensional pollutant dispersion model in an isolated street canyon. Atmos. Environ. 36, 861–872.
Chen, Q., Ren, J., Guo, Z., 2008. Field synergy analysis and optimization of decontamination ventilation designs. Int. J. Heat Mass Tran. 51, 873–881.
Cheng, W., Liu, C., Leung, D., 2008. Computational formulation for the evaluation of street canyon ventilation and pollutant removal performance. Atmos. Environ. 42, 9041–9051.
Cui, P.Y., Li, Z., Tao, W.Q., 2017. Numerical investigations on Re-independence for the turbulent flow and pollutant dispersion under the urban boundary layer with some experimental validations. Int. J. Heat Mass Tran. 106, 422–436.
Ding, S., Huang, Y., Cui, P., Wu, J., Li, M., Liu, D., 2019. Impact of viaduct on flow reversion and pollutant dispersion in 2D urban street canyon with different roof shapes - numerical simulation and wind tunnel experiment. Sci. Total Environ. 671, 976–991.
Dong, J., Tan, Z., Xiao, Y., 2017. Seasonal changing effect on airflow and pollutant dispersion characteristics in urban street canyons. Atmosphere 8, 43.
Dou, H., Ming, T., Li, Z., Peng, C., Zhang, C., Fu, X., 2018. Numerical simulation of pollutant dispersion characteristics in a three-dimensional urban traffic system. Atmospheric Pollution Research 9, 735–746.
Du, Y., Blocken, B., Pirker, S., 2020. A novel approach to simulate pollutant dispersion in the built environment: transport-based recurrence CFD. Build. Environ. 170, 106604.
Gu, Z., Zhang, Y., Cheng, Y., Lee, S., 2011. Effect of uneven building layout on air flow and pollutant dispersion in non-uniform street canyons. Build. Environ. 46, 2657–2665.
Guo, Z., Li, D., Wang, B., 1998. A novel concept for convective heat transfer enhancement. Int. J. Heat Mass Tran. 41, 2221–2225.
Hamid, M., Zhang, B., Yang, L., 2014. Application of field synergy principle for optimization fluid flow and convective heat transfer in a tube bundle of a pre-heater. Energy 76, 241–253.
Hang, J., Luo, Z., Wang, X., He, L., Wang, B., Zhu, W., 2017. The influence of street layouts and viaduct settings on daily carbon monoxide exposure and intake fraction in idealized urban canyons. Environ. Pollut. 220, 72–86.
Hang, J., Wang, Q., Chen, X., Sandberg, M., Zhu, W., Buccolieri, R., 2015. City breathability in medium density urban-like geometries evaluated through the pollutant transport rate and the net escape velocity. Build. Environ. 94, 166–182.
Hang, J., Xian, Z., Wang, D., Mak, C., Wang, B., Fan, Y., 2018. The impacts of viaduct settings and street aspect ratios on personal intake fraction in three-dimensional urban-like geometries. Build. Environ. 143, 138–162.
Hang, J., Buccolieri, R., Yang, X., 2019. Impact of indoor-outdoor temperature differences on dispersion of gaseous pollutant and particles in idealized street canyons with and without viaduct settings. Building Simulation 12, 285–297.
Hao, C., Xie, X., Huang, Y., Huang, Z., 2019. Study on influence of viaduct and noise barriers on the particulate matter dispersion in street canyons by CFD modeling. Atmospheric Pollution Research 10, 1723–1735.
Hideki, K., Ryozo, O., Mengtao, H., Keigo, N., 2018. Consistency of mean wind speed in pedestrian wind environment analyses: mathematical consideration and a case study using large-eddy simulation. J. Wind Eng. Ind. Aerod. 173, 91–99.
Huang, Y., He, W., Kim, C., 2015. Impacts of shape and height of upstream roof on airflow and pollutant dispersion inside an urban street canyon. Environ. Sci. Pollut. Res. Int. 22, 2117–2137.
Jicha, M., Pospisil, J., Katolicky, J., 2000. Dispersion of pollutants in street canyon under traffic induced flow and turbulence. Environ. Monit. Assess. 65, 343–351.
Kastner, P., Berkowicz, R., Britter, R., 2004. The influence of street architecture on flow and dispersion in street canyons. Meteorol. Atmos. Phys. 87, 121–131.
Kato, S., Ito, K., Murakami, S., 2003. Analysis of visitation frequency through particle tracking method based on LES and model experiment. Indoor Air 13, 182–193.
Keigo, N., Ryozo, O., Hideki, K., 2018. Evaluation of k-ε Reynolds stress modeling in an idealized urban canyon using LES. J. Wind Eng. Ind. Aerod. 175, 213–228.
Kim, J.-J., Baik, J.-J., 2004. A numerical study of the effects of ambient wind direction on flow and dispersion in urban street canyons using the RNG k–ε turbulence model. Atmos. Environ. 38, 3039–3048.
Li, X.-X., Liu, C., Leung, D.Y., 2008. Large-eddy simulation of flow and pollutant dispersion in high-aspect-ratio urban street canyons with wall model. Boundary-Layer Meteorol. 129, 249–268.
Li, Z., Shi, T., Wu, Y., Zhang, H., Juan, Y., Ming, T., Zhou, N., 2020. Effect of traffic tidal flow on pollutant dispersion in various street canyons and corresponding mitigation strategies. Energy and Built Environment 1, 242–253.
Li, Z., Xu, J., Ming, T., Peng, C., Huang, J., Gong, T., 2017. Numerical simulation on the effect of vehicle movement on pollutant dispersion in urban street. Procedia Engineering 205, 2303–2310.
Lin, L., Hang, J., Wang, X., Wang, X., Fan, S., Fan, Q., 2016. Integrated effects of street layouts and wall heating on vehicular pollutant dispersion and their reentry toward downstream canyons. Aerosol and Air Quality Research 16, 3142–3163.
Liu, C.-H., Leung, D.Y., Barthm, M.C., 2005. On the prediction of air and pollutant exchange rates in street canyons of different aspect ratios using large-eddy simulation. Atmos. Environ. 39, 1567–1574.
Liu, W., Liu, Z., Ma, L., 2012. Application of a multi-field synergy principle in the performance evaluation of convective heat transfer enhancement in a tube. Chin. Sci. Bull. 57, 1600–1607.
Liu, W., Liu, Z.C., Huang, S.Y., 2010. Physical quantity synergy in the field of turbulent heat transfer and its analysis for heat transfer enhancement. Chin. Sci. Bull. 55, 2589–2597.
Liu, Z., Liu, W., Nakayama, A., 2007. Flow and heat transfer analysis in porous wick of CPL evaporator based on field synergy principle. Heat Mass Tran. 43, 1273–1281.
Lu, C., Cao, L., Norback, D., Li, Y., Chen, J., Deng, Q., 2019. Combined effects of traffic air pollution and home environmental factors on preterm birth in China. Ecotoxicol. Environ. Saf. 184, 109639.
Mei, S.-J., Luo, Z., Zhao, F.-Y., Wang, H.-Q., 2019. Street canyon ventilation and airborne pollutant dispersion: 2-D versus 3-D CFD simulations. Sustainable Cities and Society 50, 101700.
Merah, A., Noureddine, A., 2019. Reactive pollutants dispersion modeling in a street canyon. Int. J. Appl. Mech. Eng. 24, 91–103.
Michioka, Tl, Sato, A., Takimoto, H., Kanda, M., 2011. Large-eddy simulation for the mechanism of pollutant removal from a two-dimensional street canyon. Boundary-Layer Meteorol. 138, 195–213.
Mochida, A., Tominaga, Y., Murakami, S., Yoshie, R., Ishihara, T., Ooka, R., 2002. Comparison of various k-ε models and DSM applied to flow around a high-rise building—report on AIJ cooperative project for CFD prediction of wind environment. Wind Struct. 5 (2–4), 227–244.
Nicholson, S.E.A., 1975. Pollution model for street-level air. Atmos. Environ. 9, 19–31.
Nowak, D.J., Crane, D.E., Stevens, J.C., 2006. Air pollution removal by urban trees and shrubs in the United States. Urban For. Urban Green. 4, 115–123.
Pavageau, M., Schatzmann, M., 1999. Wind tunnel measurements of concentration fluctuations in an urban street canyon. Atmos. Environ. 33, 3961–3971.
Solazzo, E., Cai, X., Vardoulakis, S., 2008. Modelling wind flow and vehicle-induced turbulence in urban streets. Atmos. Environ. 42, 4918–4931.
Soulhac, L., Perkins, R.J., Salizzoni, P., 2008. Flow in a street canyon for any external wind direction. Boundary-Layer Meteorol. 126, 365–388.
Su, J., Wang, L., Gu, Z., Song, M., Cao, Z., 2019. Effects of real trees and their structure on pollutant dispersion and flow field in an idealized street canyon. Atmospheric Pollution Research 10, 1699–1710.
Shirasawa, T., Tominaga, T., Yoshie, R., Mochida, A., Yoshino, H., Kataoka, H., Nozu, T., 2003. Development of CFD method for predicting wind environment around a high-rise building part 2: the cross comparison of CFD results using various k- models for the flowfield around a building model with 4:4:1 shape. AIJ J.Technol. Des. 18, 169–174 (in Japanese).
Takano, Y., Moonen, P., 2013. On the influence of roof shape on flow and dispersion in an urban street canyon. J. Wind Eng. Ind. Aerod. 123, 107–120.
Tallis, M., Taylor, G., Sinnett, D., Freer-Smith, P., 2011. Estimating the removal of atmospheric particulate pollution by the urban tree canopy of London, under current and future environments. Landsc. Urban Plann. 103, 129–138.
Tan, Z., Dong, J., Xiao, Y., Tu, J., 2015. Numerical simulation of diurnally varying thermal environment in a street canyon under haze-fog conditions. Atmos. Environ. 119, 95–106.
Tan, Z., Tan, M., Sui, X., Jiang, C., Song, H., 2019. Impact of source shape on pollutant dispersion in a street canyon in different thermal stabilities. Atmospheric Pollution Research 10, 1985–1993.
Tao, W.-Q., Guo, Z.-Y., Wang, B.-X., 2002. Field synergy principle for enhancing convective heat transfer—its extension and numerical verifications. Int. J. Heat Mass Tran. 45, 3849–3856.
Wang, H., Chen, Q., 2012. A new empirical model for predicting single-sided, wind-driven natural ventilation in buildings. Energy Build. 54, 386–394.
Wang, P., Dai, G., 2018. Field synergy of the rod bank on the enhancement of mass transfer in a spray column. Ind. Eng. Chem. Res. 57, 12531–12542.
Wang, C.H., Li, Q., Wang, Z.H., 2018. Quantifying the impact of urban trees on passive pollutant dispersion using a coupled large-eddy simulation–Lagrangian stochastic model. Build. Environ. 145, 33–49.
Wang, Q., Fang, W., de, Richter R., Peng, C., Ming, T., 2019. Effect of moving vehicles on pollutant dispersion in street canyon by using dynamic mesh updating method. J. Wind Eng. Ind. Aerod. 187, 15–25.
Wu, X.M., Yu, Y.S., Zhang, C.Y., Wang, G.X., Feng, B., 2014. Identifying the CO2 capture performance of CaCl2-supported amine adsorbent by the improved field synergy theory. Ind. Eng. Chem. Res. 53, 10225–10237.
Xie, X., Huang, Z., Wang, J., 2005a. Impact of building configuration on air quality in street canyon. Atmos. Environ. 39, 4519–4530.
Xie, X., Huang, Z., Wang, J., Xie, Z., 2005b. The impact of solar radiation and street layout on pollutant dispersion in street canyon. Build. Environ. 40, 201–212.
Yan, K., Ge, P., Hu, R., Meng, H., 2012. Heat transfer and resistance characteristics of conical spiral tube bundle based on field synergy principle. Chin. J. Mech. Eng. 25, 370–376.

Zeng, M., Tao, W.-Q., 2004. Numerical verification of the field synergy principle for turbulent flow. J. Enhanc. Heat Transf. 11, 453–460.

Zhong, J., Cai, X.M., Bloss, W.J., 2015. Modelling the dispersion and transport of reactive pollutants in a deep urban street canyon: using large-eddy simulation. Environ. Pollut. 200, 42–52.

Zhong, J., Cai, X.M., Bloss, W.J., 2017. Large eddy simulation of reactive pollutants in a deep urban street canyon: coupling dynamics with O_3-NO_x-VOC chemistry. Environ. Pollut. 224, 171–184.

Zhou, J.-J., Wu, Z.-G., Tao, W.-Q., 2006. Numerical simulation and field synergy analysis of heat transfer performance of radial slit fin surface. Prog. Comput. Fluid Dynam. Int. J. 6, 419–427.